RESEARCH ARTICLE

Aggregate WILEY

Unconventional assemblies of bisacylhydrazones: The role of water for circularly polarized luminescence

Hye Jin Cho[1] | **Dong Yeun Jeong[2]** | **Hwihyun Moon[1]** | **Taewoo Kim[1]** |
You Kyoung Chung[1] | **Yeongdong Lee[3]** | **Zonghoon Lee[3]** | **Joonsuk Huh[1]** |
Youngmin You[2] | **Changsik Song[1]**

[1] Department of Chemistry, Sungkyunkwan University, Suwon, Gyeonggi 16419, Republic of Korea

[2] Division of Chemical Engineering and Materials Science, Graduate Program in System Health Science and Engineering, Ewha Womans University, Seoul 03760, Republic of Korea

[3] Center for Multidimensional Carbon Materials, Institute for Basic Science (IBS), Department of Materials Science and Engineering, Ulsan National Institute of Science and Technology (UNIST), Ulsan 44919, Republic of Korea

Correspondence
Changsik Song, Department of Chemistry, Sungkyunkwan University, 2066 Seobu-ro, Janangu, Suwon, Gyeonggi, 16419, Republic of Korea.
Email: songcs@skku.edu

Abstract
Understanding the precise molecular arrangement of chiral supramolecular polymers is essential not only to comprehend complex superstructures like proteins and DNA but also for the development of next-generation optoelectronic materials, including materials displaying high-performance circularly polarized luminescence (CPL). Herein, we report the first chiral supramolecular polymer systems based on hydrazone–pyridinium conjugates comprising alkyl chains of different lengths, which afforded control of the apparent supramolecular chirality. Although supramolecular chirality is governed basically by the remote chiral centers of alkyl chains, helicity inversion was achieved by controlling the conditions under which the hydrazone building blocks underwent aggregation (i.e., solvent compositions or temperature). More importantly, the addition of water to the system led to aggregation-induced hydrazone deprotonation, which resulted in a completely different self-assembly behavior. Structural water molecules played an essential role, forming the assembly's channel-like backbone, around which hydrazone molecules gathered as a result of hydrogen bonding interactions. Further co-assembly of an achiral hydrazone luminophore with the given supramolecular polymer system allowed the fabrication of a novel CPL-active hydrazone-based material exhibiting a high maximum value for the photoluminescence dissymmetry factor of -2.6×10^{-2}.

KEYWORDS
circularly polarized luminescence (CPL), helicity control, hydrazone, self-assembly, structural water, supramolecular polymerization

1 | INTRODUCTION

Chirality is a fundamental characteristic of natural systems found at various levels, from the subatomic and molecular levels to the macroscopic scale. Some of the best examples of chirality are found in biological systems: L-amino acids, D-sugars, the right-handed α-helix of proteins, and the right-handed double helix of DNA. Notably, chirality at the supramolecular level—that is the chirality of self-assembled systems—has become the focus of substantial research interest, because it affects the further formation of superstructures responsible for complex biological functions, such as target recognition and catalysis.[1] Against this backdrop, the field of supramolecular chemistry has been rapidly developing, given that it is closely related to molecular self-assembly, and its study enables us to better understand biological systems and construct biomimetic systems.[2]

Defined by Lehn, supramolecular chemistry is a field of chemistry dealing with complex species composed of two or more individual molecules kept together by noncovalent interactions.[3,4] Beyond the biological context, integration between the academic disciplines of supramolecular chemistry and polymer science resulted in a whole new type of polymer called supramolecular polymer,[5] which possesses beneficial functional properties such as reversibility,[6–9] adaptability,[10] self-healing,[11,12] and responsiveness to stimuli.[13] Endowing supramolecular systems with chirality allows materials to be used in various fields, including sensing, catalysis, optical switches, memory, and optoelectronic devices.[1,2,14]

One emerging utility of chiral supramolecular systems is circularly polarized luminescence (CPL). An electromagnetic wave consists of an oscillating electric field and an oscillating magnetic field that is perpendicular to each other, moreover, the direction of the oscillation of the electric field is referred to as the direction of polarization. Natural light is composed of electromagnetic waves that are polarized in all directions randomly, so it is overall unpolarized. However, CPL is the phenomenon whereby photoluminescence exhibits stronger intensity along the direction of left-handed circular polarization than that along the direction of right-handed circular polarization, or vice versa. When CPL-active materials are placed in a dissymmetric environment and are photoexcited, they produce such circularly polarized emissions.[2,15] CPL has drawn much attention, because of the potential for it to be exploited in state-of-the-art studies in various research fields, such as 3D displays,[16–19] optical sensors,[20–22] optoelectronic devices,[23–25] and quantum information processing.[26–28] The CPL performance is characterized by a photoluminescence dissymmetry factor (g_{lum}), a normalized value of differential CPL intensities.[29–31] Although a number of chiral materials exhibiting CPL activity have been reported, developing such materials that are characterized by a high g_{lum} has become a key goal for their practical use.[31,32] Recent research work aimed at developing ideal CPL candidates has focused on organic systems, particularly self-assembling ones.[30,33,34] Even achiral luminophores can develop CPL as a result of a self-assembly process taking place in a dissymmetric environment; specifically, this goal is mostly achieved via the incorporation into the supramolecular assembly of chiral host materials or the application of external forces (e.g., vortex flow).[35–37] In such an approach, various organic emitters can be utilized, ensuring efficient progress in CPL-active materials.

We recently reported the development of *bis*-hydrazone–pyridinium conjugates (**BH**s), which form one-dimensional nanowires through the supramolecular polymerization process.[38] Helical nanowires were created in this case while the building blocks were self-assembled by direct intermolecular interaction; however, helicity control was not achieved. Herein, we report **BH**s substituted with chiral alkyl chains, which self-assembled preferentially in a particular direction, affording helicity control. Importantly, this supramolecular chirality could be inverted by tuning environmental conditions such as solvent composition or building block aggregation temperature. More interestingly, by adding water, **BH**s were observed to form co-assemblies comprising water through hydrogen bonding interactions (Scheme 1). This network of chiral **BH**s that include structural water molecules exhibits strong CPL. We previously reported the aggregation-induced emission (AIE) properties of a hydrazone-based achiral fluorophore (**BAH-1**) that were turned on or off by the reversible adsorption of water molecules.[39] Adopting **BH**s as a chiral platform, we successfully generated CPL from **BAH-1** by forming a co-assembly with **BH**s under conditions whereby water could be added. The thus generated CPL exhibited a maximum $|g_{lum}|$ value of 2.6×10^{-2}, which is comparable to the amplified CPL obtained in self-assembled systems of previous works.[40–44] Although the exact mechanism through which **BH**s successfully transferred their own chirality to **BAH-1** has not yet been clarified, the structural characteristics of the single-crystals of a model compound of **BH**s emphasized the importance of the hydrogen bonding network of the water molecules as the driving force of the formation of the co-assembled structure.

2 | RESULTS AND DISCUSSION

A series of **BH**s substituted with alkyl chains were synthesized via condensation of hydrazide derivatives and 4-pyridinecarboxaldehyde followed by nucleophilic substitution with *p*-xylylene dibromide (Figure 1A). In order to determine how the identity of the alkyl chain affects the shape of the supramolecular **BH**-based polymer, we compared the scanning electron microscopy (SEM) images and circular dichroism (CD) spectra of **BH**s comprising different alkyl chain substituents drop-casted on a glass substrate. Based on the SEM images, the presence of a long alkyl chain seemed to lead to the formation of uniformly shaped helical wires. Indeed, the shortest **BH**, **BH1** (i.e., no alkyl substituent groups), formed short nanosheets, but compounds from **BH4** to **BH7**, which have alkyl chains at their termini, successfully self-assembled to form helical wires (see Figure 1B,C and Figure S1).

Another significant factor affecting the shape of self-assembled **BH** wires was observed to be the chirality of the alkyl substituents. Similar to what was observed in previous studies on helical supramolecular assemblies,[45–47] we found that the chirality of alkyl substituents determined the overall supramolecular helicity. A negative Cotton effect was observed in the CD spectrum of the film of *S,S*-**BH5**, which comprises (*S*)-2-methylbutoxy groups as substituents; by contrast, a positive Cotton effect was observed in the CD of *R,R*-**BH5** (Figure 1D,E). In addition, it seems that the CD spectrum of *S,S*-**BH5** might have two Cotton effects, first at 360 nm and second at 305 nm. However, considering that only one Cotton effect was observed in the CD spectrum of *R*-isomer, we assumed this change was not a Cotton effect, in which the inversion of signal occurred due to the baseline shifting. The same divergence in helicity was also observed in SEM images: supramolecular assemblies obtained with *S* chiral alkyl chains exhibited *M* helicity, while supramolecular assemblies obtained with *R* chiral alkyl chains exhibited *P* helicity (Figure 1B,C). In transmission electron microscopy (TEM) images, oblong **BH** nanosheets were visible, which in part rolled up (Figure S2). The evidence thus suggests that the longer the alkyl chains are, the longer also are the nanosheets. At the same time, solvent vaporization induces the scrolling of nanosheets; as a result, helical nanowires are observed.[48] We assume that the terminal chirality tilts the overall alignment of the molecules in nanosheets, so that only one helicity may be favored.

In order to understand the relationship between molecular arrangement and observed helicity, the CD spectra of chiral monohydrazones *S*-**H5** and *R*-**H5** were calculated (Figure S3). Based on the antiparallel stacking structure of the monohydrazone model compound of our previous work,[38] we designed the stacked model compounds with terminal alkyl chains. In order to determine the local geometries of model compounds, we performed density functional theory calculations using a hybrid functional B3LYP and 6–311++G** basis set implemented in Gaussian 16 program.[49] Further
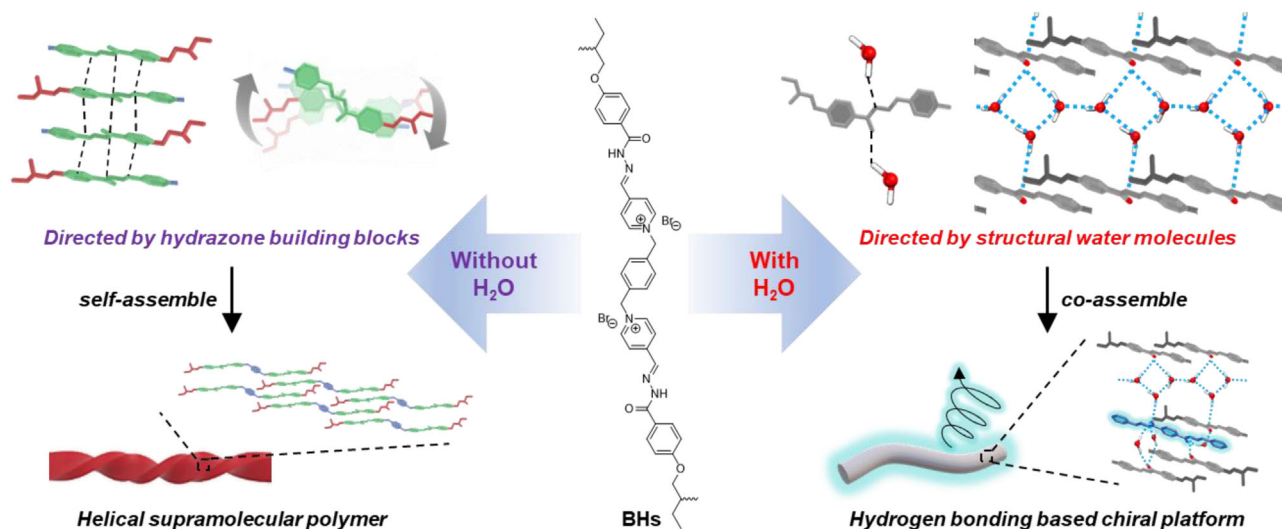
SCHEME 1 Pathways of supramolecular polymerization of bis-p-pyridinium benzoyl hydrazone in different environments
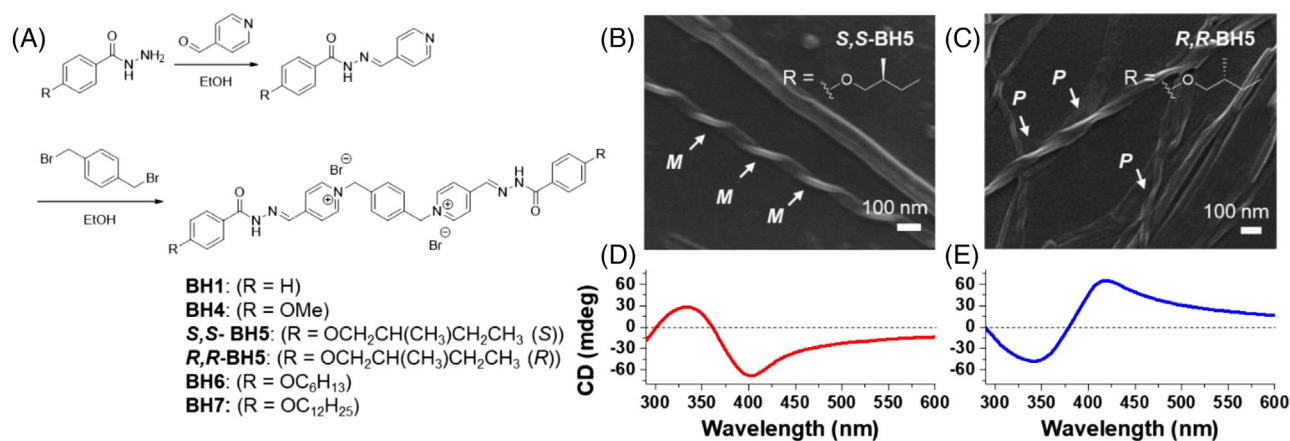

FIGURE 1 (A) Synthesis of alkyl-substituted hydrazone–pyridinium conjugates. (B,C) Scanning electron microscopy images of bis-hydrazones (1.0×10^{-4} M in methanol) whose termini were substituted with (B) an *S*-chiral alkyl group (*S,S*-BH5) or (C) an *R*-chiral alkyl group (*R,R*-BH5). Approximately 10 μL of each solution was drop-casted on the glass, which was subsequently dried under vacuum. (D,E) Circular dichroism (CD) spectra of *S,S*-BH5 (D) and *R,R*-BH5 (E); a BH5 1.0×10^{-3} M solution in methanol was utilized to record the CD spectra (50 μL of the solution was drop-casted on the glass; glass size: 1.1×4.0 cm^2). EtOH: ethanol; Me: methyl

optimizations were carried out using the Turbomole 7.3 program with def2-SVP basis set to observe the molecular stacking behavior of *S*-H5 and *R*-H5 in the six-layered form with a tilt angle of ~10°, respectively. According to the simulated structures, the two model compounds tended to stack in opposite directions. The alkyl chain with *S* chirality in *S*-H5 induced the central chromophores to stack on top of each other in an anticlockwise direction, while the alkyl chain with *R* chirality induced the central chromophores to stack in a clockwise direction. Moreover, the calculated CD spectra appeared to be in good agreement with the experimental CD spectra of BH5s, corroborating the idea that terminal chirality controls the arrangement of central chromophores.

A more in-depth investigation of the chiral supramolecular polymerization process was then conducted using *S,S*-BH5, and *R,R*-BH5 solutions in methanol/toluene co-solvent systems. A small amount of HCl was also added to the co-solvent systems to prevent the appearance of a charge transfer (CT) band by deprotonation, which is a typical absorption band appearing in a merocyanine-type dye.[50,51] The aggrega-

tion process was monitored by UV–Visible (UV–Vis) absorption and CD spectroscopy as the proportion of toluene in the co-solvent system was made to increase. BH5 molecules are readily dissolved in methanol, so they tend to exist in monomeric form until the toluene proportion increases above the value of 95% (v/v). At a methanol/toluene volume ratio of 3/97, *S,S*-BH5 exhibited a negative Cotton effect, while *R,R*-BH5 exhibited a positive Cotton effect (Figure 2A,B), similarly to the CD spectra recorded in films.

Interestingly, a rapid inversion of chirality was observed in the CD spectra when the sample was prepared in a solvent characterized by a methanol/toluene volume ratio of 1/99. Using *S,S*-BH5, the solvent-induced chirality inversion was also observed at higher *S,S*-BH5 concentrations (35 and 50 μM; Figure S4). However, the overall shape of the UV–Vis absorption spectra of BH5s in methanol/toluene = 1/99 appeared almost identical to that of BH5s in methanol/toluene = 3/97 or films (Figures S4 and S5). The evidence thus suggests that only the molecular stacking changed the other way around (i.e., helicity inversion
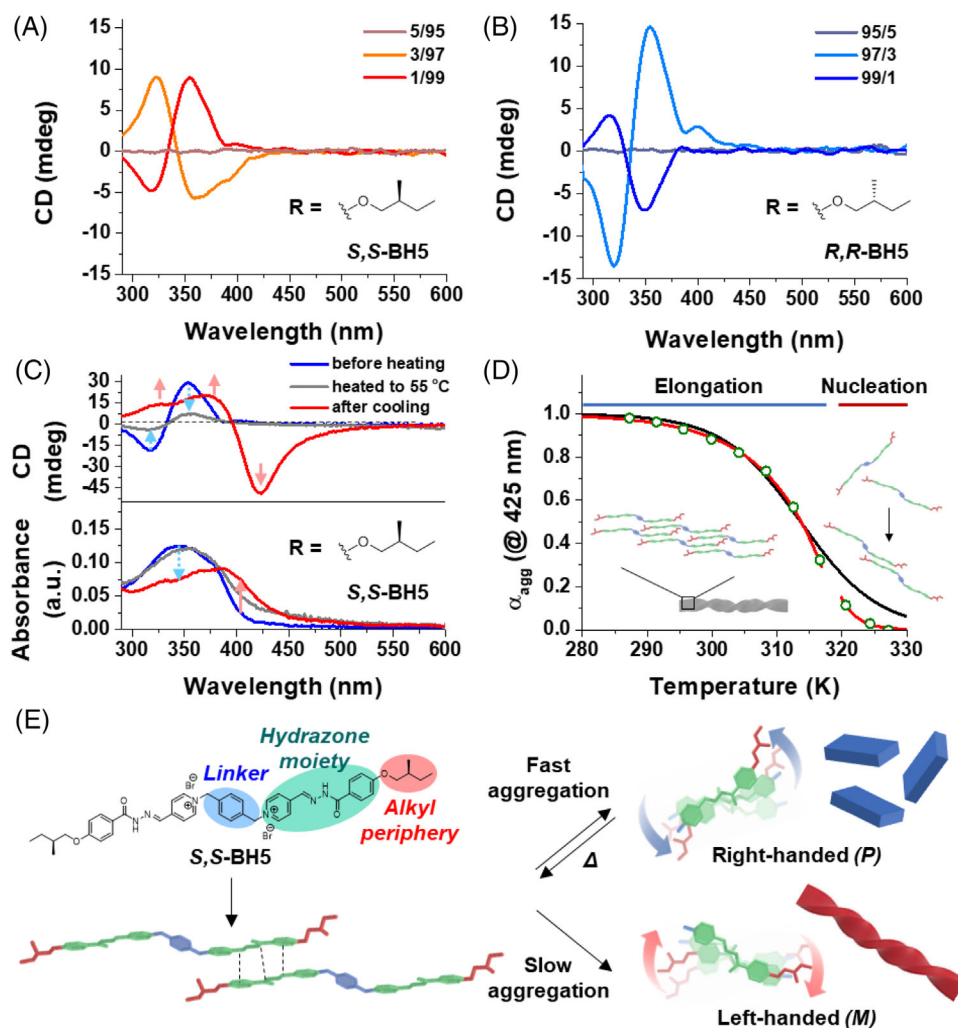
FIGURE 2 (A,B) Solvent-induced supramolecular chirality inversion observed by circular dichroism (CD) spectrometry in the case of 2.0×10^{-5} M solutions of (A) *S,S*-BH5 and (B) *R,R*-BH5 in methanol/toluene (v/v = 5/95, 3/97, and 1/99) in the presence of HCl. (C) Temperature-induced change of absorption and CD spectra observed for *S,S*-BH5 (5.0×10^{-5} M in methanol/toluene = 1/99), before (blue line), and after (red line) the heating-cooling process. Notably, the solution was heated to 55°C for ~7 min, at which time the spectrum of the solution was recorded (gray line); the solution was then slowly cooled to 14°C at a rate of 2 K/min. (D) The plot of the value of the fraction of aggregates (α_{agg}) *versus* the temperature; the plot also includes the theoretical lines for the isodesmic (black line) and cooperative (red line) model of supramolecular polymerization. (E) Schematic representation of how the kinetically or thermodynamically controlled supramolecular polymers of *S,S*-BH5 could be formed

occurred) at high **BH5** concentrations or under fast aggregation conditions. According to SEM evidence, **BH5**s prepared in similar conditions consisted of short nanosheets (Figure S6).

We performed temperature-dependent CD studies on *S,S*-**BH5** to gain an in-depth understanding of the mechanism of supramolecular polymerization (Figure 2C,D). When the temperature of the *S,S*-**BH5** solution in methanol/toluene = 1/99 was made to increase up to 55°C, the CD signal was significantly diminished. The remaining positive signal totally disappeared by further heating, and the inversed Cotton effect of a strong negative signal was observed after slowly cooling the solution to 14°C (cooling rate: 2 K/min). The same phenomenon was observed to occur at various *S,S*-**BH5** concentrations (Figure S7). Considering all these changes, we assume that the inversion of chirality observed in temperature-dependent CD measurements was due to the disassembly of the kinetically favored aggregates, followed by the formation of the thermodynamically favored supramolecular polymer (Figure 2E). The aggregation rate seems thus to play an important role in determin-

ing the type of product. At a methanol/toluene volume ratio of 1/99, *S,S*-**BH5** monomers are kinetically trapped by the fast aggregation process. On the other hand, at higher values for the methanol content of the co-solvent system, the monomers tend to aggregate slowly and form the most stable assemblies—i.e., the thermodynamically favored species forms. In addition, the kinetically favored aggregates are much shorter than their thermodynamically favored counterparts, presumably due to the unfavorable molecular arrangement (Figure S6). Using *R,R*-**BH5**, we observed that the exact opposite CD signals appeared when the same experiments were conducted. Since the transition from the kinetic product (obtained in methanol/toluene = 1/99) to the thermodynamic product (obtained implementing the heating-cooling process) works via a monomeric state, determining the amount of energy supplied to the system during the disassembly process would be important to predict the product obtained after cooling. We varied the heating time from 10 to 40 min, and we found the resulting two products to exhibit different CD spectra (Figure S8). The sample that had been heated for a shorter period of time displayed a CD spectrum

with the exact shape in which the thermodynamic and kinetic products co-exist. By contrast, the sample heated for a longer period of time was demonstrated to consist of the thermodynamic product, supporting our hypothesis on the transition between kinetic and thermodynamic products.

We further investigated the cooling curves obtained from the temperature-dependent CD studies. First, we observed the gradual disassembly of S,S-BH5 brought about by heating through monitoring the CD signal at 353 nm (Figure S9A). During the slow cooling process, we monitored the CD signal at 425 nm and observed the formation of the thermodynamic product (Figure S9B). The α_{agg} value was calculated from the cooling curve and plotted as a function of the temperature (Figure 2D). Unlike the results of our previous study,[38] the development of a supramolecular polymer using S,S-BH5 could be described well by the nucleation–elongation model,[52,53] rather than by the isodesmic model, indicating that the monomers had assembled cooperatively in the present case. Based on the simulation performed using the nucleation–elongation model, T_e, and K_a were calculated to have values of ∼320 K and 3.0×10^{-3}, respectively. Representative examples of cooperative supramolecular polymerization usually exhibit nearly ten times lower K_a values (Table S1). Our system exhibits a gentle onset of elongation regime, with a higher K_a value than those previously reported, which refers to a lower degree of cooperativity ($\approx K_a^{-1/3}$). Our system is comparable to those reported for bis(merocyanine) dyes (K_a of $1.22–1.46 \times 10^{-3}$).[54]

Next, we replaced toluene with water in the co-solvent system. In this case, we did not add HCl to the solvent mixture because the system seemed to include enough protons. The water molecules seemed to engage in hydrogen bonding interactions with hydrazone molecules, and, surprisingly, the aggregation process facilitated the removal of the acidic proton of the hydrazone (Figure 3A). This aggregation-induced deprotonation is uncommon; in fact, the present observation is the first such case reported for hydrazone. The light yellow color of the methanol solution, due to the presence of S,S-BH5 in the monomeric state, became orange as a result of the addition of water (Figure 3B,C). One could assume that this change is due to the charge transfer induced by water. However, the CT band of the hydrazones showed hypsochromic shifts with solvent polarity, similar to that of Brooker's merocyanine dye.[38] We confirmed the formation of the zwitterionic form of S,S-BH5, which we named S,S-BQ5, by analyzing the orange precipitates isolated from the suspension. Indeed, in the ^{1}H-NMR spectra of the orange precipitates, the resonances due to the aromatic protons of the pyridinium ring (H_b and H_c) were observed to shift upfield with respect to those of as-is powder, along with resonances due to the imine (H_d) and benzyl (H_h) protons (Figure 3D). More importantly, the resonance due to the acidic proton (H_a) disappeared altogether, indicating that the orange precipitate consisted of S,S-BQ5. The characteristics of the UV–Vis absorption (Figure S10) and Fourier-transform infrared (FT-IR) (Figure S11) spectra of three different powders (as-is, precipitates obtained from methanol/water, and deprotonated powder) prepared using S,S-BH5, and external base also support the formation of S,S-BQ5 in the methanol/water co-solvent system.

We also monitored the changes in the UV–Vis absorption and CD spectra of a S,S-BH5 solution as a result of the progressive addition of water to it (Figure 3E). Until the water proportion in the co-solvent system remained below 70%, the spectra remained unchanged. Once the said value was reached, the intensity of the absorption peak due to the monomer at 348 nm decreased dramatically; moreover, a new absorption peak at 510 nm appeared as a result of the further addition of water (methanol/water = 1/9). These changes in the absorption spectra were accompanied by the opacification of the solution and by the appearance of a CD signal, which suggested that S,S-BH5 aggregation was the driving force of the deprotonation. Notably, the same phenomena were observed in the case of R,R-BH5, while no CD signals were observed for the racemic mixture of S,S-BH5, and R,R-BH5 (rac-BH5; Figure S12).

Deprotonated hydrazones could still self-assemble into wires (Figure S13). In this case, it seemed obvious that the molecular arrangement and intermolecular interactions contributing to the supramolecular polymerization process would differ from that of BH1. In order to further investigate how the alkyl-substituted hydrazones aggregate in the presence of water, single crystals of the model compound H4 were grown in a basic aqueous solution (Figure 4A). The deprotonated H4, dubbed Q4, formed two types of crystals: needle-shaped (Figure S14) and flat diamond-shaped (Figure S15). The needle-shaped crystals belonged to the $P2_1/c$ space group, whereby the molecules were packed in a zigzag arrangement (Figure S14B). In the needle-shaped crystals, both the O and N atoms of the amide moiety (O=C–N) of hydrazone participated in hydrogen bonding interactions with water molecules, resulting in a lengthened C=O bond (1.25 Å) compared to H1 (1.21 Å).[38] On the other hand, in the case of the flat diamond-shaped crystals (P-1 space group), only the O atom engaged in hydrogen bonding interactions with water molecules. Owing to the electron donation from the free N atom to the O atom, the C–N bond appeared to be slightly shorter in the flat diamond-shaped crystals than in the needle-shaped crystals (1.34 Å vs. 1.36 Å), while the C=O bond appeared to be longer (1.27 Å).

We assumed that the supramolecular polymerization would follow the molecular arrangement of the needle-shaped crystals since these crystals were much more abundant than the flat diamond-shaped ones. Interestingly, we found a hydrogen-bonding network of "structural water" molecules (Figure 4B). Unlike H1 molecules, which stacked as a result of direct intermolecular interactions, the water molecules acted as essential co-monomers forming the network that plays the role of the backbone of the structure and gathered Q4 molecules around the periphery of the said backbone as a result of hydrogen bonding interactions. The assembly resembles that of mosaic viruses and other monomers coated on their surface.[55] Organic materials whereby structural water molecules drive the material's self-assembly have been rarely reported.[56–58] In fact, to the best of our knowledge, the present study represents the first reported case of water-driven self-assembly achieved solely using hydrazone derivates, in a system, in other words, that did not include any metal ions, which are known to form Metallo-supramolecular assemblies with water and ligand molecules.[59,60]

According to the evidence from the crystal structure, neighboring Q4 molecules aligned in a complex fashion with one another. The two adjacent Q4 molecules not connected to each other by hydrogen bonds were positioned antiparallel to each other, similarly to what was observed
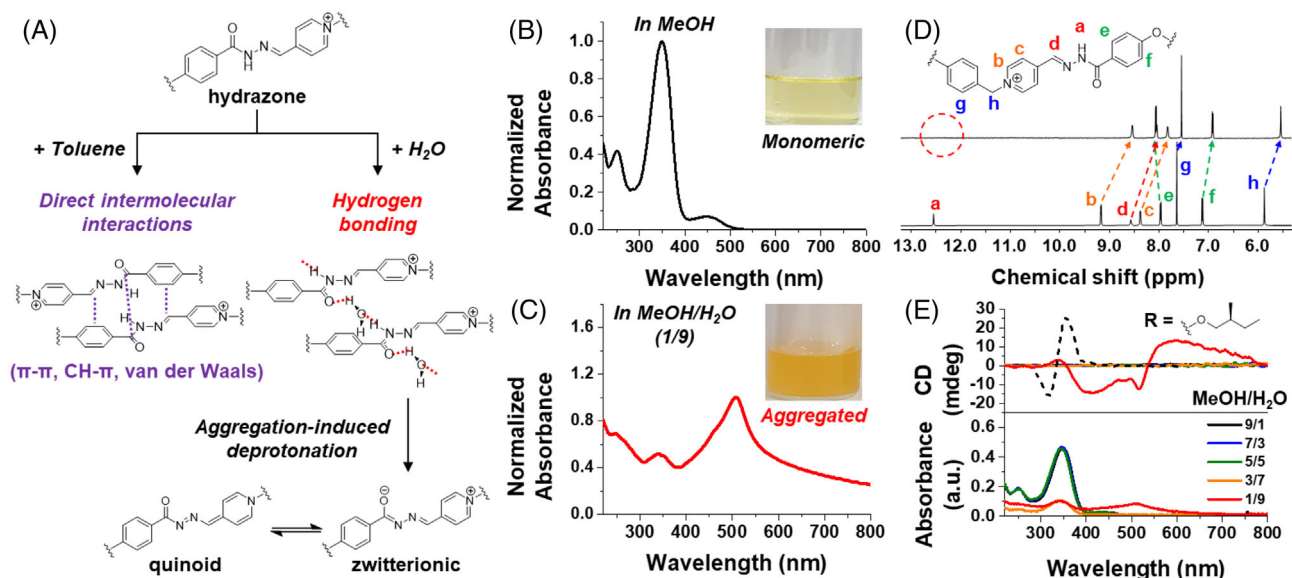
FIGURE 3 (A) Schematic representation of how the intermolecular interactions of the hydrazone chromophore change as a result of the addition of water. (B,C) Absorption spectra of a *S,S*-BH5 1.0×10^{-4} M solution in (B) pure methanol (MeOH) and (c) in a 1/9 (v/v) MeOH/water co-solvent system. Insets: photos of the corresponding solutions. (D) ^{1}H-NMR spectra of *S,S*-BH5 comparing the as-is powder (down) and precipitates collected from MeOH/water (1/9) solution (up). Each sample was dissolved in DMSO-*d6*. (E) Absorption and circular dichroism (CD) spectra of solutions of *S,S*-BH5 in MeOH/water (1.0×10^{-4} M) as the proportion of water in the co-solvent system increased from 10% to 90%. The CD spectrum of *S,S*-BH5 in MeOH/toluene (5.0×10^{-5} M) is also plotted for comparison (black dashed line)
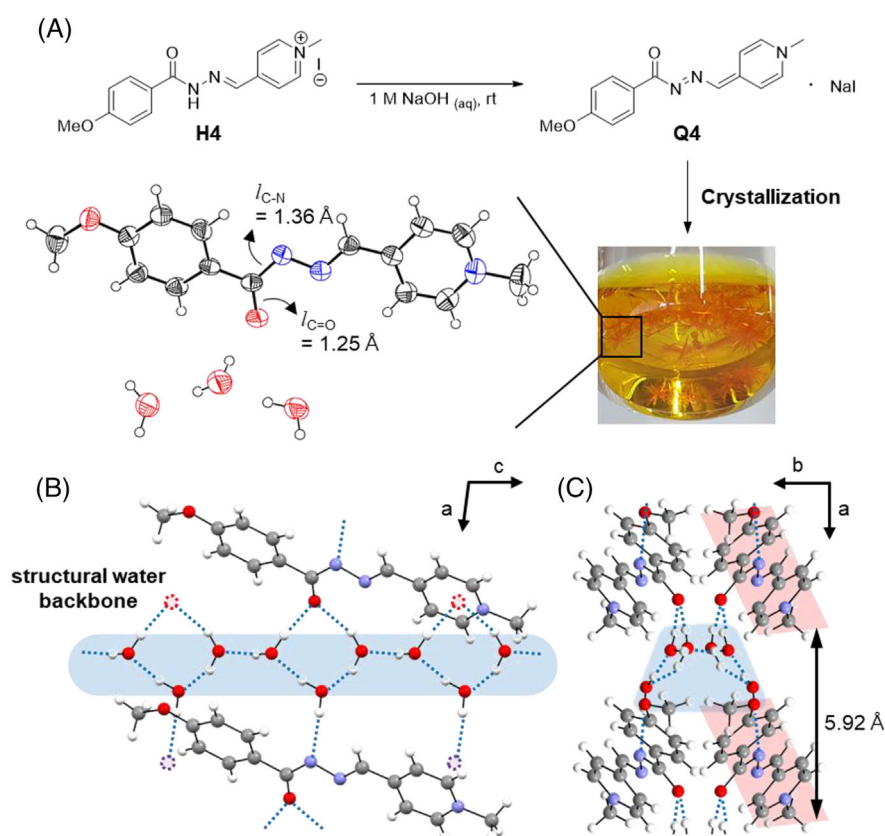

FIGURE 4 (A) Synthesis of single crystals using model compound **Q4**. (B,C) Two-dimensional crystal packing arrangements, viewed along the (B) b-axis and (C) c-axis. Notably, some O and N atoms of certain **Q4** molecules are represented as dotted circles, while the rest of the structure is removed for clarity

for **H1** molecules. However, the two adjacent **Q4** molecules bound through structural water molecules were observed to be arranged in parallel to each other (Figure 4C). These two parallel molecules are relatively far apart; the distance

between the two planes containing each hydrazone is 5.92 Å. The presence of such a large void prevents direct intermolecular interactions so that the **Q4** molecules interact only through the hydrogen bonds with the water backbone. In addition,
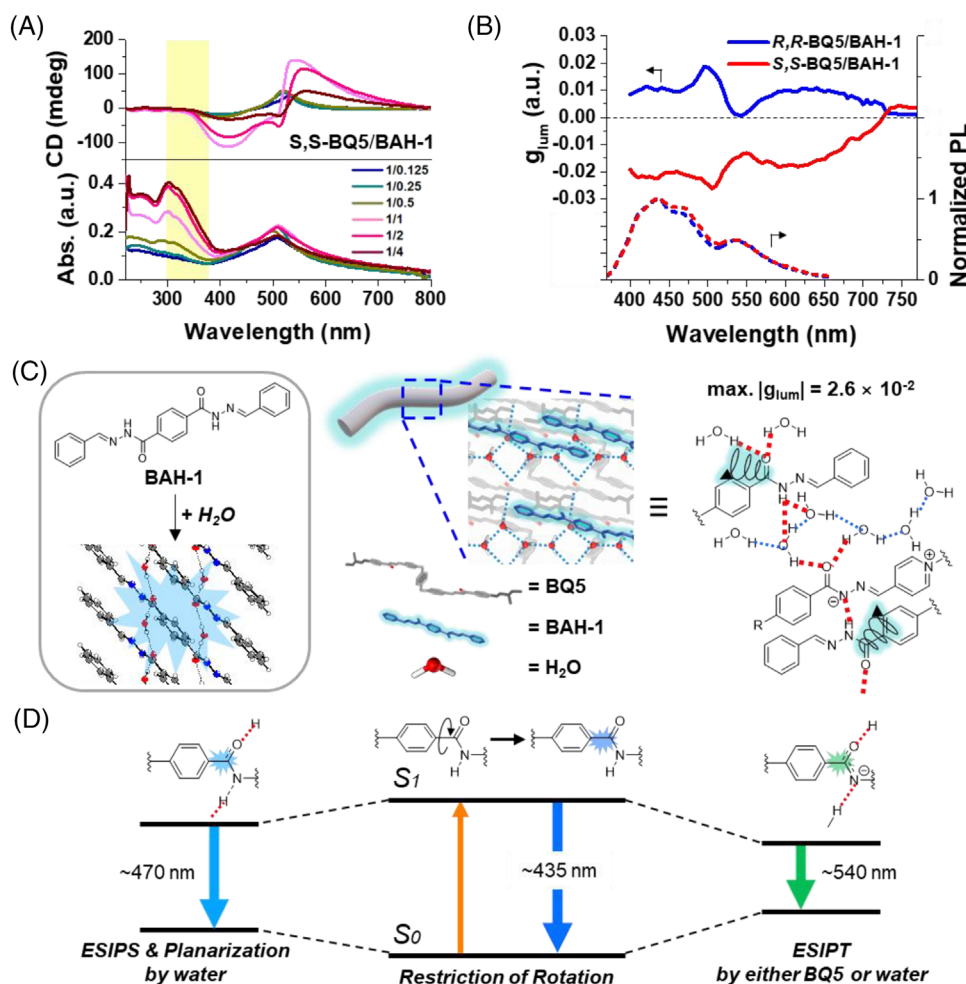
FIGURE 5 Chirality transfer from **BQ5** to the achiral fluorophore **BAH-1**. (A) Absorption and circular dichroism (CD) spectra of **S,S-BQ5** (1.0×10^{-4} M) co-assembled with **BAH-1** (from 0.125 to 4 equiv. with respect to **S,S-BQ**) in methanol/water (1:9 v/v). (B) Circularly polarized luminescence (CPL) spectra of **(S,S)-1**, which consisted of **S,S-BQ5** (1.0×10^{-4} M) co-assembled with **BAH-1** (1 equiv.) in methanol/water (1:9 v/v), plotted with photoluminescence (PL) spectra below. PL sepctra were excited at the wavelength of 340 nm. (C) Schematic illustration of the co-assembly of **BQ5** and **BAH-1** (left: aggregation-induced emission of **BAH-1** Ref. [39]). (D) Schematic representation of the proposed mechanism for dual emission in **BAH-1**. ESIPS: excited-state interlayer proton shift; ESIPT: excited-state interlayer proton transfer; g_{lum}: luminescence dissymmetry factor

the lengths of the N–N bond of the hydrazone moiety and the C=C bonds of the pyridinium ring did not change meaningfully. Notably, the polar environment and intermolecular hydrogen bonding interactions appeared to favor the localization of the charge and to favor the zwitterionic form.

Finally, we utilized the supramolecular polymers of **BQ5**s as chiral platforms for generating CPL, with an achiral hydrazone luminophore, **BAH-1**. Hydrazone has been rarely used in CPL-active materials,[61,62] although its derivatives exhibit aggregation-induced emission (AIE) activities.[39] We first confirmed that the supramolecular chirality observed in **S,S-BH5** preserved in the co-assembled system **(S,S)-1**, which consists of **S,S-BQ5**, and **BAH-1** (Figure 5A). SEM images of **(S,S)-1** proved that the system maintained a wire-type assembly (Figure S16). The intensity of the CD signal of **(S,S)-1** was more than 10 times as large as the intensities of the CD signals of **S,S-BH5** and **S,S-BQ5** (Figure S17A). Considering that the supramolecular chirality arises as a result of the aggregation of individual molecules, it is obvious that **BAH-1** molecules facilitated the formation of aggregated species by lowering their solubility. Here, we used dimethyl sulfoxide (DMSO) as the solvent to dissolve the **BAH-1** to the desired concentration while preparing **(S,S)-1**. In order to confirm that the solvent does not lead to CD signal amplifi-

cation, we used pure DMSO instead of the **BAH-1** solution for the co-assembly process, and we observed that adding a small amount of DMSO did not induce any significant change in the CD spectrum of **S,S-BH5** (Figure S17B).

We further investigated the emission spectrum of **(S,S)-1** (Figure 5B). The emission spectrum was similar to that of **BAH-1** in our previous report,[39] which demonstrated that the hydrogen bonding between **BAH-1** and water molecules effectively restricts the intramolecular rotation (RIR)[63] and facilitates the excited-state interlayer proton shift (ESIPS),[64] resulting in dual emission. Interestingly, a new emission band at around 540 nm was also observed, which we will discuss later. Photoluminescence excitation (PLE) measurements conducted on the systems confirmed that the UV–Vis absorption of **BAH-1** in the hydrogen bonding network (at ~350 nm; highlighted in Figure 5A) is the main contributor to the observed emission (Figure S18). Notably, no new Cotton effects were observed in this absorption region, leading us to assume that the **BAH-1** molecules themselves would not be closely spaced to each other for exciton coupling. Although we could not find direct evidence of a chirality transfer from the **BQ5**–water network to **BAH-1** in the CD spectra, the occurrence of this transfer is assured by the strong CPL signals with a maximum g_{lum} value of

-2.6×10^{-2}. Comparing the signs of CD and CPL observed in them, we found the inversion of sign; the CPL signal is positive when a negative Cotton effect is observed in the CD spectrum, and the CPL signal is negative when the system is characterized by a positive Cotton effect. Regarding these opposite signs of CD and CPL spectra, we suppose that the CD spectra reveal the ground state chirality while the CPL spectra reveal that of the excited state. Even though the absolute PL quantum yield (PLQY) was lower than 0.1%, the g_{lum} value was relatively high and comparable to those of CPL-amplified systems previously reported.[40–44] **(R,R)-1** was prepared to utilize **R,R-BQ5** in place of **S,S-BQ5**. The two systems exhibited mirror-image CPL signals in the emission region.

Considering that the structural water molecules formed the backbone of the assembly, we propose the schematic illustration of which **BAH-1** molecules were placed near the **BQ5** or water molecules of the backbone (Figure 5C). The location and shape of the first and second emission bands of **(S,S)-1** are identical to the corresponding bands in the emission spectrum of **BAH-1**, which has been aggregated under the water.[39] Based on this observation, we were able to infer that the first emission peak at 435 nm arose as a result of the reinforced RIR process, while the second peak at 470 nm arose as a result of the ESIPS occurring between **BAH-1** and water molecules. For the new emission band (at ~540 nm), we propose the transfer of protons—i.e., the occurrence of an excited-state intermolecular proton transfer (ESIPT)[65]— instead of a proton shift to explain the appearance of the third emission band (Figure 5D). Note that **BAH-1** is able to form hydrogen bonds not only with the water molecules but also with the amide moiety of **BQ5**. The negatively charged amide moiety of **BQ5** would strongly attract the protons of **BAH-1**, leading to their transfer in the excited state. The S1 state of lower energy would then be generated, and, as a result, the third emission band appears. The interaction between **BAH-1** and **BQ5** would ensure the successful transfer of the chirality from the platform to the doped chromophore, resulting in a distinct emission spectrum with a strong CPL character.

3 | CONCLUSION

We synthesized a series of hydrazone–pyridinium conjugates (**BH**s), which self-assembled into helical nanowires. The hydrazone building blocks with chiral alkyl substituents exhibited a single helicity by chiral spatial arrangement induced by the chiral substituents. On further investigation of the formation of these helical supramolecular polymers, we determined that changing solvent composition or the thermal energy balance could change the appearance of the polymers' CD spectra. Through mechanistic investigations, we inferred that two types of products are involved in the change: the thermodynamically-favored and kinetically-favored products. Interestingly, upon the addition of water, deprotonation of the hydrazone chromophore was accompanied by an aggregation process. Based on structural data obtained from the single crystals of the model compound **Q4**, we were able to conclude that water molecules participated in the assembly process acting as structural molecules. Notably, we successfully fabricated a chiral system from **BH5** and water molecules, which exhibited CPL with a high g_{lum}

value of -2.6×10^{-2} when further co-assembled with the achiral luminophore **BAH-1**. The results of our study on the supramolecular polymerization of **BH**s afforded us an in-depth understanding of the self-assembly of hydrazone derivatives. The evidence collected provides further opportunities to develop advanced chiral platforms, which could be applied to the manufacture of functional soft materials.

CONFLICT OF INTEREST
There are no conflicts to declare

ETHICS STATEMENT
There are no ethical issues in this work.

DATA AVAILABILITY STATEMENT
The data that supports the findings of this study are available within the article and in the Supporting Information of this article. The Supporting Information is available free of charge at https://doi.org/10.1002/agt2.168.

REFERENCES
1. E. Yashima, N. Ousaka, D. Taura, K. Shimomura, T. Ikai, K. Maeda, *Chem. Rev.* **2016**, *116*, 13752.
2. M. H. Liu, L. Zhang, T. Y. Wang, *Chem. Rev.* **2015**, *115*, 7304.
3. J. M. Lehn, *Science* **1985**, *227*, 849.
4. J. M. Lehn, *Angew. Chem. Int. Ed.* **1988**, *27*, 89.
5. B. Qin, Z. H. Yin, X. Y. Tang, S. Zhang, Y. H. Wu, J. F. Xu, X. Zhang, *Prog. Polym. Sci.* **2020**, *100*, 101167.
6. M. K. Muller, L. Brunsveld, *Angew. Chem. Int. Ed.* **2009**, *48*, 2921.
7. M. Takeshita, M. Hayashi, S. Kadota, K. H. Mohammed, T. Yamato, *Chem. Commun.* **2005**, 761.
8. B. Yu, B. Wang, S. Guo, Q. Zhang, X. Zheng, H. Lei, W. Liu, W. Bu, Y. Zhang, X. Chen, *Chem. Eur. J.* **2013**, *19*, 4922.
9. T. Haino, T. Fujii, A. Watanabe, U. Takayanagi, *Proc. Natl. Acad. Sci.* **2009**, *106*, 10477.
10. K. Liu, Y. Kang, Z. Wang, X. Zhang, *Adv. Mater.* **2013**, *25*, 5530.
11. N. Roy, B. Bruchmann, J.M. Lehn, *Chem. Soc. Rev.* **2015**, *44*, 3786.
12. L. M. de Espinosa, G. L. Fiore, C. Weder, E. J. Foster, Y. C. Simon, *Prog. Polym. Sci.* **2015**, *49-50*, 60.
13. X. Yan, F. Wang, B. Zheng, F. Huang, *Chem. Soc. Rev.* **2012**, *41*, 6042.
14. F. R. Keene, *Chirality in Supramolecular Assemblies: Causes and Consequences*. John Wiley & Sons, **2016**.
15. J. Li, X. Peng, C. Huang, Q. Qi, W. Y. Lai, W. Huang, *Polym. Chem.* **2018**, *9*, 5278.
16. D. Y. Kim, *J. Korean Phys. Soc.* **2006**, *49*, 505.
17. X. Gao, Y. Xu, J. Huang, Z. Hu, W. Zhu, X. Yi, L. Wang, *Optics Letters* **2021**, *46*, 2666.
18. L. L. Huang, X. Z. Chen, H. Muhlenbernd, H. Zhang, S. M. Chen, B. F. Bai, Q. F. Tan, G. F. Jin, K. W. Cheah, C. W. Qiu, J. S. Li, T. Zentgraf, S. Zhang, *Nat. Commun.* **2013**, *4*, 2808.
19. X. Zhan, F. F. Xu, Z. Zhou, Y. Yan, J. Yao, Y. S. Zhao, *Adv. Mater.* **2021**, *33*, 2104418.
20. H. Maeda, Y. Bando, K. Shimomura, I. Yamada, M. Naito, K. Nobusawa, H. Tsumatori, T. Kawai, *J. Am. Chem. Soc.* **2011**, *133*, 9266.
21. Y. Imai, Y. Nakano, T. Kawai, J. Yuasa, *Angew. Chem. Int. Ed.* **2018**, *57*, 8973.

22. M. C. Heffern, L. M. Matosziuk, T. J. Meade, *Chem. Rev.* **2014**, *114*, 4496.

23. Z. G. Wu, H. B. Han, Z. P. Yan, X. F. Luo, Y. Wang, Y. X. Zheng, J. L. Zuo, Y. Pan, *Adv. Mater.* **2019**, *31*, 1900524.

24. J. J. Cheng, F. Ge, C. Zhang, Y. Kuai, P. H. Hou, Y. F. Xiang, D. G. Zhang, L. Z. Qiu, Q. J. Zhang, G. Zou, *J. Mater. Chem. C* **2020**, *8*, 9271.

25. Y. J. Zhang, T. Oka, R. Suzuki, J. T. Ye, Y. Iwasa, *Science* **2014**, *344*, 725.

26. E. Karimi, B. Piccirillo, E. Nagali, L. Marrucci, E. Santamato, *Appl. Phys. Lett.* **2009**, *94*, 231124.

27. C. Wagenknecht, C. M. Li, A. Reingruber, X. H. Bao, A. Goebel, Y. A. Chen, Q. A. Zhang, K. Chen, J. W. Pan, *Nat. Photonics* **2010**, *4*, 549.

28. J. F. Sherson, H. Krauter, R. K. Olsson, B. Julsgaard, K. Hammerer, I. Cirac, E. S. Polzik, *Nature* **2006**, *443*, 557.

29. T. H. Zhao, J. L. Han, P. F. Duan, M. H. Liu, *Acc. Chem. Res.* **2020**, *53*, 1279.

30. Y. Sang, J. Han, T. Zhao, P. Duan, M. Liu, *Adv. Mater.* **2020**, *32*, 1900110.

31. F. Y. Song, Z. Zhao, Z. Y. Liu, J. W. Y. Lam, B. Z. Tang, *J. Mater. Chem. C* **2020**, *8*, 3284.

32. J. Li, C. Hou, C. Huang, S. Xu, X. Peng, Q. Qi, W. Y. Lai, W. Huang, *Research* **2020**, 3839160.

33. X. H. Tang, D. D. Chu, H. Jiang, W. Gong, C. Jiang, Y. Cui, Y. Liu, *Mater. Chem. Front.* **2020**, *4*(9), 2772.

34. K. Ma, W. J. Chen, T. F. Jiao, X. Jin, Y. T. Sang, D. Yang, J. Zhou, M. H. Liu, P. F. Duan, *Chem. Sci.* **2019**, *10*, 6821.

35. Y. T. Sang, D. Yang, Z. C. Shen, P. F. Duan, M. H. Liu, *J. Phys. Chem. C* **2020**, *124*, 17274.

36. K. Okano, M. Taguchi, M. Fujiki, T. Yamashita, *Angew. Chem. Int. Ed.* **2011**, *50*, 12474.

37. J. Q. Liang, P. P. Guo, X. J. Qin, X. H. Gao, K. Ma, X. F. Zhu, X. Jin, W. W. Xu, L. X. Jiang, P. F. Duan, *ACS Nano* **2020**, *14*, 3190.

38. K. S. Kim, H. J. Cho, J. Lee, S. Ha, S. G. Song, S. Kim, W. S. Yun, S. K. Kim, J. Huh, C. Song, *Macromolecules* **2018**, *51*, 8278.

39. H. J. Cho, K. S. Kim, H. Kim, T. Kim, A. G. Malyutin, D. C. Rees, B. K. Yoo, C. Song, *ACS Appl. Mater. Inter.* **2021**, *13*, 7546.

40. A. Mukherjee, S. Ghosh, *Chem. Eur. J.* **2020**, *26*, 12874.

41. D. Yang, P. F. Duan, L. Zhang, M. H. Liu, *Nat. Commun.* **2017**, *8*, 15727.

42. J. Ma, Y. X. Wang, X. J. Li, L. Yang, Y. W. Quan, Y. X. Chen, *Polymer* **2018**, *143*, 184.

43. L. K. Ji, Y. T. Sang, G. H. Ouyang, D. Yang, P. F. Duan, Y. Q. Jiang, M. H. Liu, *Angew. Chem. Int. Ed.* **2019**, *58*, 844.

44. Z. G. Suo, X. L. Hou, J. Q. Chen, X. W. Liu, Y. Liu, F. F. Xing, Y. Y. Chen, L. Y. Feng, *J. Phys. Chem. C* **2020**, *124*, 21094.

45. L. Brunsveld, A. P. H. J. Schenning, M. A. C. Broeren, H. M. Janssen, J. A. J. M. Vekemans, E. W. Meijer, *Chem. Lett. 29*, **2000**, 292.

46. M. Tanaka, T. Ikeda, J. Mack, N. Kobayashi, T. Haino, *J. Org. Chem.* **2011**, *76*, 5082.

47. Y. Nakano, T. Hirose, P. J. M. Stals, E. W. Meijer, A. R. A. Palmans, *Chem. Sci.* **2012**, *3*, 148.

48. X. P. Cui, Z. Z. Kong, E. L. Gao, D. Z. Huang, Y. Hao, H. G. Shen, C. A. Di, Z. P. Xu, J. Zheng, D. B. Zhu, *Nat. Commun.* **2018**, *9*, 1301.

49. M. J. Frisch, G. W. Trucks, H. B. Schlegel, G. E. Scuseria, M. A. Robb, J. R. Cheeseman, G. Scalmani, V. Barone, G. A. Petersson, H. Nakatsuji, X. Li, M. Caricato, A. V. Marenich, J. Bloino, B. G. Janesko, R. Gomperts, B. Mennucci, H. P. Hratchian, J. V. Ortiz, A. F. Izmaylov, J. L. Sonnenberg, Williams, F. Ding, F. Lipparini, F. Egidi, J. Goings, B. Peng, A. Petrone, T. Henderson, D. Ranasinghe, et al., *Gaussian 16 Rev. C.01*, Wallingford, CT, **2016**.

50. F. Wurthner, S. Yao, U. Beginn, *Angew. Chem. Int. Ed.* **2003**, *42*, 3247.

51. F. Wurthner, G. Archetti, R. Schmidt, H. G. Kuball, *Angew. Chem. Int. Ed.* **2008**, *47*, 4529.

52. D. H. Zhao, J. S. Moore, *Org. Biomol. Chem.* **2003**, *1*, 3471.

53. M. M. J. Smulders, A. P. H. J. Schenning, E. W. Meijer, *J. Am. Chem. Soc.* **2008**, *130*, 606.

54. G. Fernandez, M. Stolte, V. Stepanenko, F. Wurthner, *Chem. Eur. J.* **2013**, *19*, 206.

55. Y. Zhang, Y. X. Dong, J. H. Zhou, X. Li, F. Wang, *Molecules* **2018**, *23*, 2311.

56. S. Y. Dong, J. Leng, Y. X. Feng, M. Liu, C. J. Stackhouse, A. Schonhals, L. Chiappisi, L. Y. Gao, W. Chen, J. Shang, L. Jin, Z. H. Qi, C. A. Schalley, *Sci. Adv.* **2017**, *3*, eaao0900.

57. T. Li, Q. Zhang, D. D. Li, S. Y. Dong, W. X. Zhao, P. J. Stang, *ACS Appl. Mater. Inter.* **2020**, *12*, 38700.

58. N. J. Van Zee, B. Adelizzi, M. F. J. Mabesoone, X. Meng, A. Aloi, R. H. Zha, M. Lutz, I. A. W. Filot, A. R. A. Palmans, E. W. Meijer, *Nature* **2018**, *558*, 100.

59. D. Sadhukhan, M. Maiti, G. Pilet, A. Bauza, A. Frontera, S. Mitra, *Eur. J. Inorg. Chem. 2015*, **2015**, 1958.

60. Y. Singh, R. N. Patel, S. K. Patel, R. N. Jadeja, K. Patel, A. N. Patel, H. Roy, P. Kumar, R. J. Butcher, J. P. Jasinski, S. Cortijo, S. Herrero, *Polyhedron* **2021**, 200.

61. G. X. Huang, R. S. Wen, Z. M. Wang, B. S. Li, B. Z. Tang, *Mater. Chem. Front.* **2018**, *2*, 1884.

62. S. J. Jiang, J. B. Qiu, L. B. Lin, H. Y. Guo, F. F. Yang, *Dyes Pigm.* **2019**, *163*, 363.

63. J. Mei, N. L. C. Leung, R. T. K. Kwok, J.W. Y. Lam, B. Z. Tang, *Chem. Rev.* **2015**, *115*, 11718.

64. X. Li, J. Qiao, S. Y. Quek, K. P. Loh, *ACS Mater. Lett.* **2020**, *2*, 654.

65. X. Zhang, L. Guo, F. Y. Wu, Y. B. Jiang, *Org. Lett.* **2003**, *5*, 2667.

SUPPORTING INFORMATION

Additional supporting information may be found in the online version of the article at the publisher's website.